Discrete element modeling of ice loads on ship hulls in broken ice fields

JI Shunying[1]*, LI Zilin[1], LI Chunhua[2], SHANG Jie[3]

[1] Department of Engineering Mechanics, Dalian University of Technology, Dalian 116023, China

[2] National Marine Environment Forecasting Center, State Oceanic Administration, Beijing 100081, China

[3] North China Sea Marine Forecasting Center, North China Sea Branch, State Oceanic Administration, Qingdao 266033, China

©The Chinese Society of Oceanography and Springer-Verlag Berlin Heidelberg 2013

Abstract
Ice loads on a ship hull affect the safety of the hull structure and the ship maneuvering performance in ice-covered regions. A discrete element method (DEM) is used to simulate the interaction between drifting ice floes and a moving ship. The pancake ice floes are modelled with three-dimensional (3-D) dilated disk elements considering the buoyancy, drag force and additional mass induced by the current. The ship hull is modelled with 3D disks with overlaps. Ice loads on the ship hull are determined through the contact detection between ice floe element and ship hull element and the contact force calculation. The influences of different ice conditions (current velocities and directions, ice thicknesses, concentrations and ice floe sizes) and ship speeds are also examined on the dynamic ice force. The simulated results are compared qualitatively well with the existing field data and other numerical results. This work can be helpful in the ship structure design and the navigation security in ice-covered fields.
Key words: ice load, ship hull, discrete element method, broken ice

Citation: Ji Shunying, Li Zilin, Li Chunhua, Shang Jie. 2013. Discrete element modeling of ice loads on ship hulls in broken ice fields. Acta Oceanologica Sinica, 32(11): 50-58, doi: 10.1007/s13131-013-0377-2

1 Introduction

With the development of oil and gas exploitation, navigation and scientific investigation in polar regions, more attention has been paid to the structural design and maneuvering performance of ships in ice-covered waters. The determination of ice loads on a ship hull is a key issue for the ship structural design and maneuverability under various ice conditions and maneuvering performances. Normally, four typical sea ice conditions (level ice, pancake ice, ice ridge and iceberg) are considered when developing an appropriate interaction model between the ice cover and the ship hull. Crushing and bending failures of the ice cover perform obviously during the interaction (Su et al., 2010; Kujala and Arughadhoss, 2012; Suyuthi et al., 2012). The accumulation and impact of ice floes on a ship hull are distinct phenomena in pancake ice-hull interaction (Hansen and Loset, 1999a, b; Zhan et al., 2010). The penetration of a ship hull into the ice ridged area should be analyzed considering the cross section of the ice ridge for the ice ridge-hull interaction (Loset et al., 1998). A huge impact energy and a local ice pressure on a ship hull should be considered during the iceberg-ship hull interaction (Liu and Amahl, 2010; Liu et al., 2011). This study mainly investigates the ice load on a ship hull in broken ice fields.

The global ice resistance to a ship hull is one of the most important parameters to evaluate the ship maneuvering ability in broken ice fields. It is influenced by ice mechanical properties, such as floe thickness, size and concentration (Konno, 2009; Wang and Derradji-Aouat, 2011). Ship performance also affects the global ice forces. Ice loads on a ship hull have been studied for a moored ship in drifting ice, and for ship in straight running, zigzag maneuver and turning motion (Su et al., 2010; Zhan et al., 2010; Karulin and Karulina, 2011; Sawamura and Tachibana, 2011; Zhou, Riska et al., 2013). In addition, ice loads depend on the hull sizes and shapes and ocean dynamic characteristics.

With respect to numerical simulations, the finite element model (FEM) has been adopted widely to model ice pressure and global ice load for the level ice, ice ridge and iceberg (Aksnes, 2010; Su et al., 2011; Sayed and Kubat, 2011; Zhou, Su et al., 2012). However, the discrete element method (DEM) has attracted much attention in order to describe the breakup feature of ice during the ice-hull interaction. The DEM shows intrinsic advantages in the ice load calculation because of its ability to describe the discrete nature of ice structure on microscale and to model reasonably the ice breakup during the ice-hull interaction on macroscale (Shen et al., 1987; Lepparanta et al., 1990; Hansen and Loset, 1999a, b). Hansen and Loset (1999b) used a 2D disk DEM to calculate the ice load on a ship hull in broken ice fields. Karulin and Karulina (2011) also used a 2D disk element to simulate the interaction between a moored ship and pancake ice under different ice velocities. Recently, Zhan et al. (2010) and Lau et al. (2011) simulated the ice breaking and maneuvering abilities of an icebreaker with the DEM software of DECICE. Besides the interaction between the ice floe and the ship hull, the DEM has also been applied to calculate ice loads on offshore structures (Selvadurai and Sepehr, 1999; Sun and

Shen, 2012).

The reasonable construction of the sea ice floe element is important in the DEM simulation. 2D disks (Hopkins, 1998; Selvadurai and Sepehr, 1999; Xu et al., 2012) and polyhedrons (Polojarvi and Tuhkuri, 2009; Karulin and Karulina, 2011; Lau et al., 2011) have been developed. The 3D disk element, proposed by Hopkins, was used to calculate the interaction between ice and wave, and between ice and offshore structure (Hopkins and Shen, 2001; Dai et al., 2004; Sun and Shen, 2012). This element has the advantages of simple model development, high computational efficiency and high precision, and can be applied in the simulation of the interaction between ice floes and a ship hull in broken ice.

Therefore, this study aims at simulating the interaction between ice floes and a ship hull and calculating the global ice resistance to the ship hull with 3D disk element. In addition, the influences of ice conditions (current velocity and direction, ice floe size, ice thickness and concentration) and maneuvering speed are discussed.

2 Discrete element model for ice floe and ship hull

2.1 *Construction of ice floe disk element*

A dilated disk method has been presented for ice floe construction in broken ice fields (Hopkins, 2004). A 3D ice floe element is comprised with a top and bottom circular surface with radius R, and a cambered surface with radius r. The ice floe disk has a thickness of $2r$ and a diameter of $2(R+r)$, as shown in Fig. 1. To model the translation and rotation of an ice floe disk, both local and global coordinates are adopted. The local coordinate (x',y',z') is used to describe the relative gesture of each disk, and the global coordinate (x,y,z) is to determine the trajectory and relative position of each disk, as shown in Fig. 2. Here x' and y' are on the disk surface, and z' is normal to the disk surface. Both the local and global coordinates are Cartesian coordinate system following the right-handed rule. The transformation between local and global coordinates is realized through the quaternion method (Hopkins, 2004).
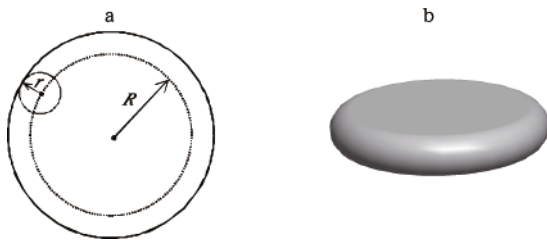
Fig.1. Construction of an ice floe with dilated disk in 3D. a. The two parameters r and R of an ice floe disk and b. an ice floe constructed with dilated disk.
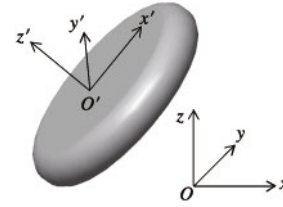
Fig.2. Local and global coordinate systems of an ice floe disk.

2.2 *Contact detection between ice floe disks*

During collisions between ice floe disks, three contact patterns can be classified as plane-plane, plane-edge and edge-edge contact, as shown in Fig. 3. Because the dilated ice floe disk is constructed with a series of spherical particles, the contact detection between disks is the determination of contacts between spherical particles. To determine the distance between two ice floe disks, an elastic band is introduced (Hopkins, 2004). Supposing the position vectors of any two arbitrary points on disk edges are r_1' and r_2' relative to the corresponding disk center, as shown in Fig. 4. An elastic band d is defined between the two points which has an elastic potential energy and makes the two spheres move on their disk edges without sliding. The elastic potential energy reaches its minimum value when the two spheres move to the positions with vectors r_1 and r_2, respectively. The distance between the two floe disks δ can thus be determined. The value of δ is negative when the two disks have an overlap during the collision.

2.3 *Contact force in ice floe collisions*

When a contact happens, the overlap between the two disks can be determined as

$$|\delta_{ij}| = |\Delta_{ij}| - (R_i + r_i) - (R_j + r_j), \tag{1}$$

where δ_{ij} is the overlap between Disk i and Disk j; $|\Delta_{ij}|$ is the distance between the two disk center; R_i, r_i and R_j, r_j are the size parameters of Disks i and j.

The contact force has normal and tangential components to the surfaces at the contact point. The normal component is

$$F_n^n = K_n \delta_{ij} - C_n V_{ij} \cdot \boldsymbol{n}, \tag{2}$$

where the subscript n denotes the normal direction; the superscript n denotes the current time step; K_n is the normal contact stiffness; C_n is the normal contact viscosity; and $\boldsymbol{v}_{ij}$ is the relative velocity of the two disks at the contact point.
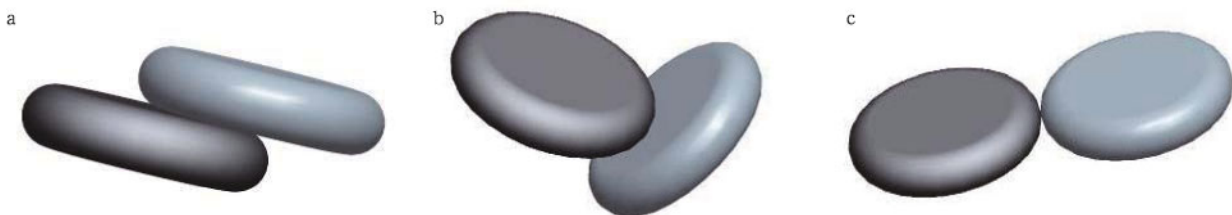
Fig.3. Three types of contacts during ice floe collisions. a. Plane-plane contact, b. plane-edge contact and c. edge-edge contact.
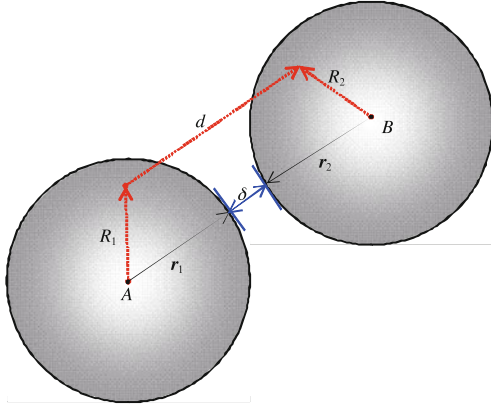
Fig.4. Contact detection with elastic band between two dilated ice floe disks.

The incremental change in the tangential force due to friction is proportional to the relative tangential velocity. The tangential force at time step n is

$$F_t^n = \min\{[F_t^{n-1} - K_t \Delta t(\boldsymbol{V}_{ij} \cdot \boldsymbol{t})], \mu F_n^n\}, \qquad (3)$$

where F_t^n and F_t^{n-1} are the tangential force at time step n and $n-1$; Δt is the time step; K_t is the tangential contact stiffness, and is set as 60% of K_n here; and μ is the inter-disk friction coefficient. Based on the Coulomb friction law, the tangential force F_t is scaled as $|F_t| = \mu F_n$ when it exceeds its limit. The torque on each ice floe can also be calculated from the contact forces.

Owing to the influences of wind and current, sea ice is subjected to the drag force and the buoyancy. The additional mass of water should also be taken into account. An ice floe in motion has different immersion depths and angles, and the infinitesimal method is used to calculate the buoyancy under different floe immersion conditions (Hopkins and Shen, 2001). The water drag force $\boldsymbol{F}_d$ on the ice floe is given by

$$\boldsymbol{F}_d = \frac{1}{2} C_d \rho_w A(\boldsymbol{V}_w - \boldsymbol{V}_i)|\boldsymbol{V}_i - \boldsymbol{V}_w|, \qquad (4)$$

where C_d is the drag coefficient of water; ρ_w is the water density; $A = \pi(R + r)^2$ is the ice floe area; and $\boldsymbol{V}_i$ and $\boldsymbol{V}_w$ are the ice floe and water velocity vectors, respectively. The drag force is separated into components normal and tangential to the flat surface of a floe. The drag coefficient C_d is 0.6 for flow normal to the flat surface and 0.06 for flow tangential to the flat surface.

The rotational drag moment is calculated in the local coordinates, and can be written as

$$\boldsymbol{M}_d = -\frac{1}{2} C_d'(R)^2 \rho_w A \boldsymbol{\omega}|\boldsymbol{\omega}|, \qquad (5)$$

where $\boldsymbol{\omega}$ is the floe rotational velocity; and C_d' is the rotational drag coefficient.

When an ice floe moves with an acceleration, its inertia force increases significantly and can be achieved with the additional mass method. The additional mass is given by

$$M_a = C_m \rho_w V_{sub} \frac{d(|\boldsymbol{V}_i - \boldsymbol{V}_w|)}{dt}, \qquad (6)$$

where M_a is the additional mass of floe ice; C_m is the additional mass coefficient and $C_m = 0.15$ here; ρ_w is the water density; and V_{sub} is the submerged area of the floe.

Under the action of water drag, inter-element force and the collision from the ship hull, the ice floes move following the Newton's second law. The quaternion method is adopted to transform the load and kinetic parameters between the local and global coordinates. The velocity and location of each floe are determined with the finite difference method at each time step.

2.4 Construction of ship hull

The ship hull can be constructed with overlapped 3D disks. Thus, the interaction between the ship hull and the ice floe can be treated as collisions between disks. The *Xuelong* icebreaker is a unique vessel for polar navigation of China, as shown in Fig. 5a. The hull has a dimension of 167 m×22.6 m×13.5 m with a draught of 9 m. The angle of the bow is 52°. We used 222 overlapped disks with the size of R=3 m and r=4 m to construct the ship hull, as shown in Fig. 5b. The hull is set as a rigid body during the interaction with ice floes.

Fig.5. *Xuelong* icebreaker in the broken ice filed and the ship hull constructed with overlapped 3D disks. a. Icebreaker *Xuelong* and b. DEM of the ship hull.

3 DEM results of ice loads on ship hull

A rectangular computational domain is used to model the broken ice field with a dimension of 600 m×250 m. Considering the random distribution of ice floes under the natural con-
dition, the ice field is filled with a single layer of ice floes with an arbitrary packing pattern with a certain concentration. The ice floe diameter R is also set as a random distribution in the range from 2.0 to 3.0 m. Considering the ice thickness parame-

ter r=0.3 m here, the ice floe diameter D, which equals $2(R+r)$, lies in the range from 4.6 to 6.6 m. The initial distribution of ice floes is shown in Figs 6 and 7a. In this study, periodic boundaries are adopted in horizontal directions, and the main computational parameters are listed in Table 1. The ship runs into the ice field from the open water with a constant velocity from the right side, and goes out from the left side.

Ship maneuvers straightly from open water with a speed of 4.0 m/s, and reaches the ice field after 7.5 s. Figures 7b, c and d are the snapshots of the interaction bewteen ice floes and the ship hull at t=20.0 s, 60.0 s and 100.0 s, respectively. The instantaneous ice resistance to the ship hull in different directions are obtained and shown in Fig. 8. In the x direction (the maneuvering direction), the maximum and mean ice load are 1 479 and 440 kN, respectively. In the y direction, the ice load has an obvious fluctuation and its mean value is about 0. The maximum ice load in the y direction is 633 kN, which is much smaller than that in the x direction. Thus, the ice load in the x direction is the key parameter for ship maneuvering straightly in broken ice fields.

4 Influences of ship speed and ice conditions on ice loads

In the following simulations, the basic computational parameters are set as ice thickness H_i=0.6 m, floe size D lies in the range from 4.6 to 6.6 m with random probability distribution, current velocity V_w=0 m/s, ship velocity V_{ship}=4.0 m/s, initial ice concentration C=60%. Other parameters are the same as listed in Table 1.

To analyze the influence of ship speed on the ice load, we set the ship speed from 1.0 to 7.0 m/s. The simulated ice loads on the hull are plotted in Fig. 9. The ice load shows obvious fluctuation under the collision of ice floes. The maximum and averaged ice loads are plotted in Fig. 10. It shows that the ice resistance increases obviously with the increasing of ship speed. The ship speed has a close relationship with the impact velocity between the ice floe and the hull. As the ship speed increases,
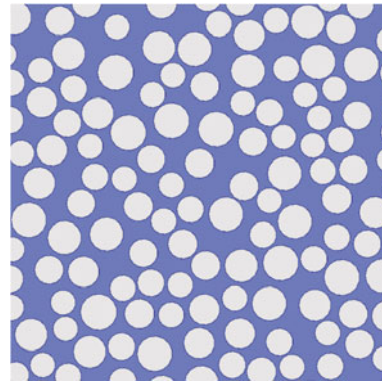
Fig.6. The random size and distribution of ice floes in the computational domain.
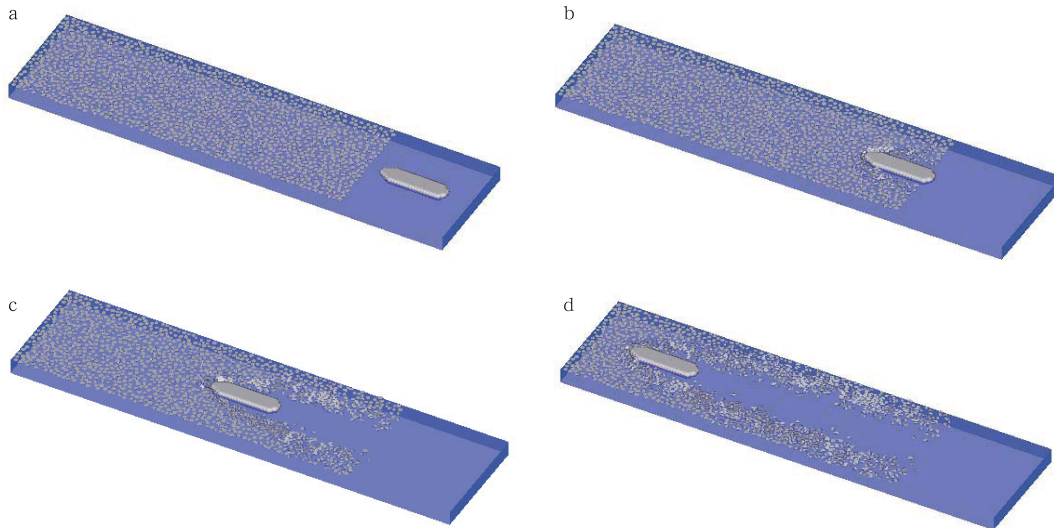
Fig.7. Snapshots of the interaction between ship hull and ice floes at different time. a. t=0 s, b. t=20.0 s, c. t=60.0 s, and d. t=100.0 s.

Table 1. Computational parameters in the DEM simulation of ice floe-ship hull interaction

Definition	Symb	Value	Definition	Symb	Value
Ice density/kg·m^{-3}	ρ_i	970	Initial ice concentration	C	0.6
Water density/kg·m^{-3}	ρ_w	1 010	Floe surface friction		0.35
Ice floe size parameter/m	R	2–3	Added mass coefficient	C_m	0.15
Ice thickness parameter/m	r	0.3	Viscous damping coefficient	ζ	0.01
Nomal contact stiffness/kN·m^{-1}	K_n	587	Ice floe number	N_p	1 600
Tangentia contact stiffness	K_t	0.6	Domain length	L_x	600
Normal drag coefficient	C_d^n	0.6	Domain width	L_y	250
Tangential drag coefficient	C_d^t	0.06	Navigational speed/m·m^{-1}	V_{ship}	4.0
Rotational drag coefficient	C_d'	0.6			
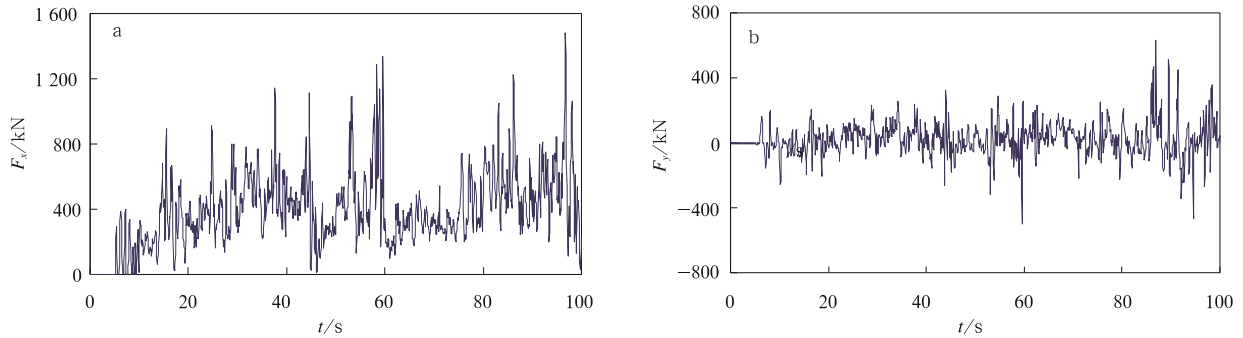
Fig.8. Dynamic ice loads on the ship hull in x and y directions. a. Ice load in the x direction and b. ice load in the y direction.
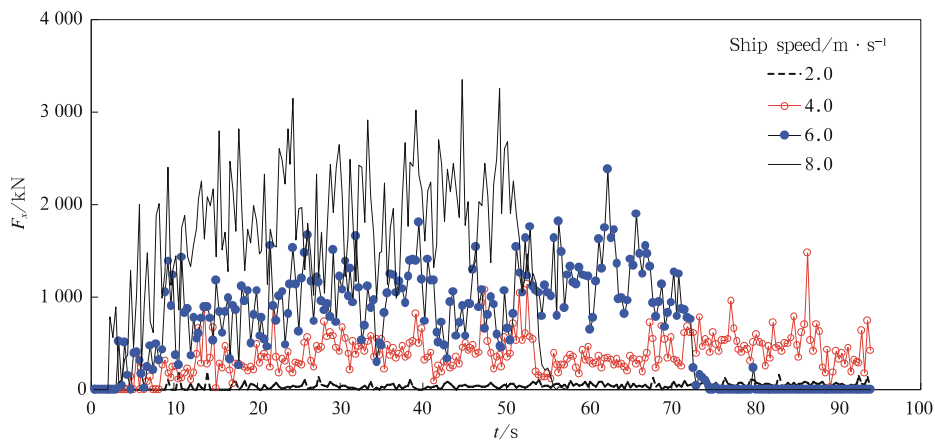
Fig.9. Time series of impact forces on ship hull under different ship speeds.
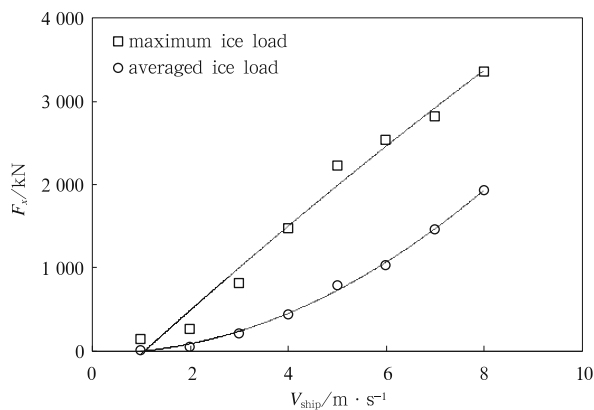
Fig.10. Maximum and mean values of ice load impacting on ship hull under different ship speeds.

the impact velocity, the kinetic energy and the contact frequency during collisions increase directly.

To analyze the influences of ice conditions, we first consider the change of the current velocity. For the moored ship, the simulated maximum and averaged ice loads are plotted in Fig. 11a under the current velocity of 0.25, 0.50, 1.00, 1.50, 2.00 m/s, respectively. For the maneuvering ship with a speed of 4.0 m/s, the simulated results are plotted in Fig. 11b. It shows that the global ice resistance increases obviously with the increase of current velocity for both cases. For the moored ship, the maximum ice load increases from 58.0 to 202.2 kN when the current

velocity increases from 0.25 to 2.00 m/s. While the mean ice resistance increases from 0.2 to 28.9 kN. For the maneuvering ship with V_{ship}=4.0 m/s, the maximum and averaged ice loads increase from 1 126.0 to 2 279.0 kN and from 409.6 to 900.3 kN, respectively. The simulated results show that the ice load is a function of the relative speed between the ice floe and the ship hull. The relative speed increases with the increase of either the current velocity or the ship speed. The ice load on ship hull increases obviously with the increase of relative speed.

Under the natural conditions, the ice drifting direction changes with tides and wind drag. The influence of current direction on the ice load is analyzed here. The ship speed is set as 4.0 m/s in the x direction, and the current direction set as 0°, 20°, 40° and 60°, respectively. The snapshots of the interaction are shown in Fig. 12. The global ice resistances in the x and y directions are plotted in Fig. 13. It shows the ice load in the x direction decreases, while the ice load in the y direction increases with the increase of current angle.

Both of the ice concentration and ice thickness are the important parameters affecting the ice load significantly. Figure 14a shows the maximum and averaged ice load on the hull under the ice concentrations of 50%, 60%, 70% and 80%, respectively. Figure 14b plots the maximum and averaged ice load when the thicknesses are in the range from 0.1 to 1.2 m, respectively. It shows that the ice load increases with the increase of ice concentration and ice thickness.

To examine the influence of ice floe size on the ice resistance to the ship hull under a constant initial ice concentration

C=60%, we set the floe size as 5, 6, 7 and 8 m, respectively. The simulated global ice resistances are plotted in Fig. 15a. It shows that the ice load is not sensitive to the ice floe size. It is known that the floe size affects the impact energy and also the contact force on the hull. With larger floe size, the impact load is larger for a single impact. Here the ice concentration remains constant, and the ice floe number decreases with the increase of ice floe size. The averaged contact force for one ice floe and the
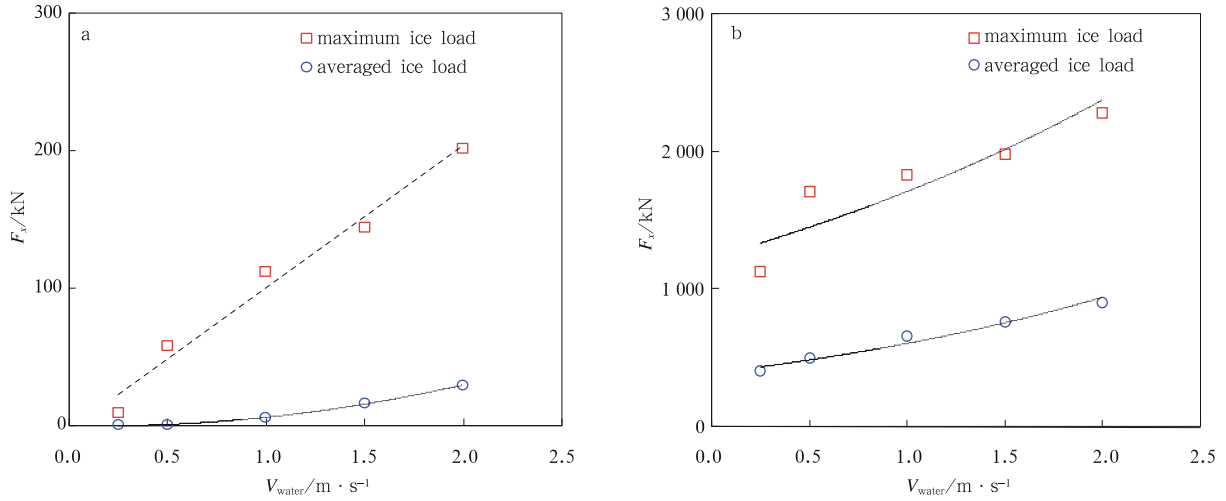
Fig.11. Maximum and mean values of ice load impacting on ship under different current velocities. a. Ice load on moored ship and b. ice load on running ship with V_{ship}=4.0 m·s^{-1}.
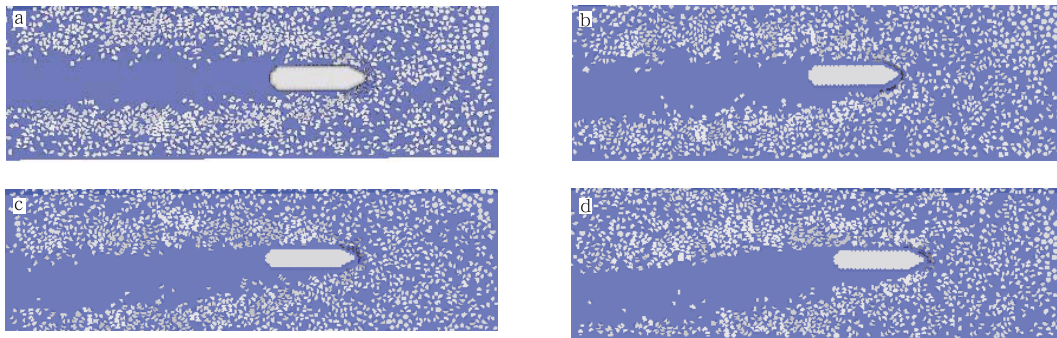
Fig.12. Snapshots of the ice floes on a maneuvering ship under different current directions. a. Current direction 0°, b. current direction 20°, c. current direction 40°, and d. current direction 60°.
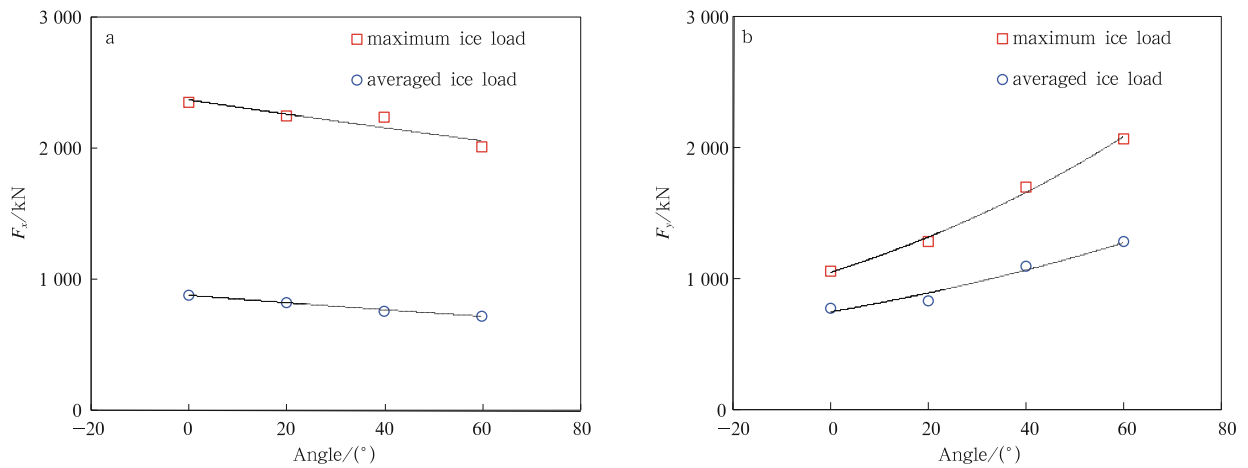
Fig.13. Influence of the current direction on ice loads on a maneuvering ship. a. Ice load in x direction and b. ice load in y direction.
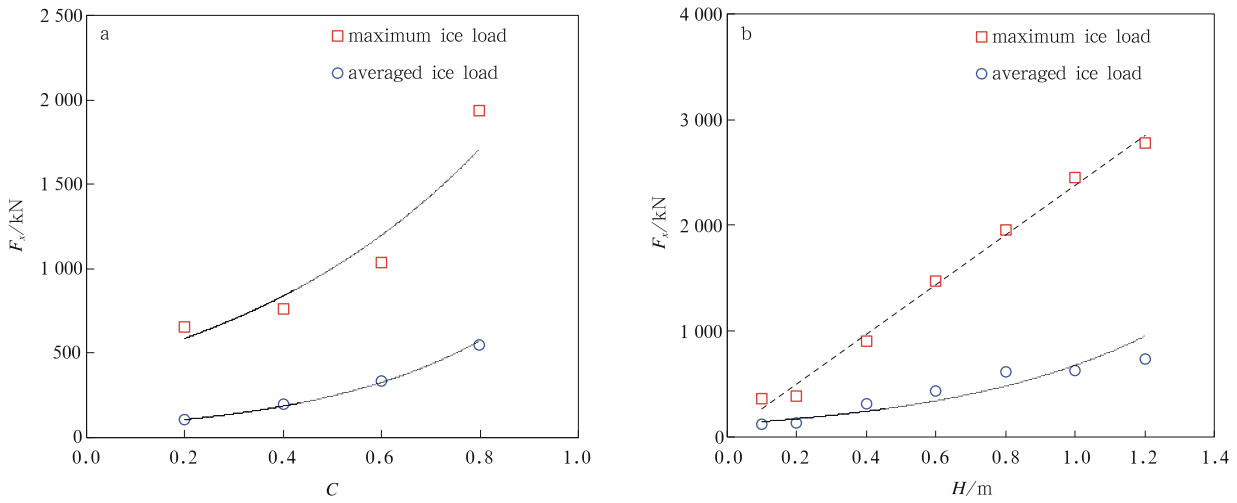
Fig.14. Maximum and mean value of ice load impacting on ship hull. a. Influence of ice concentration and b. influence of ice thickness.
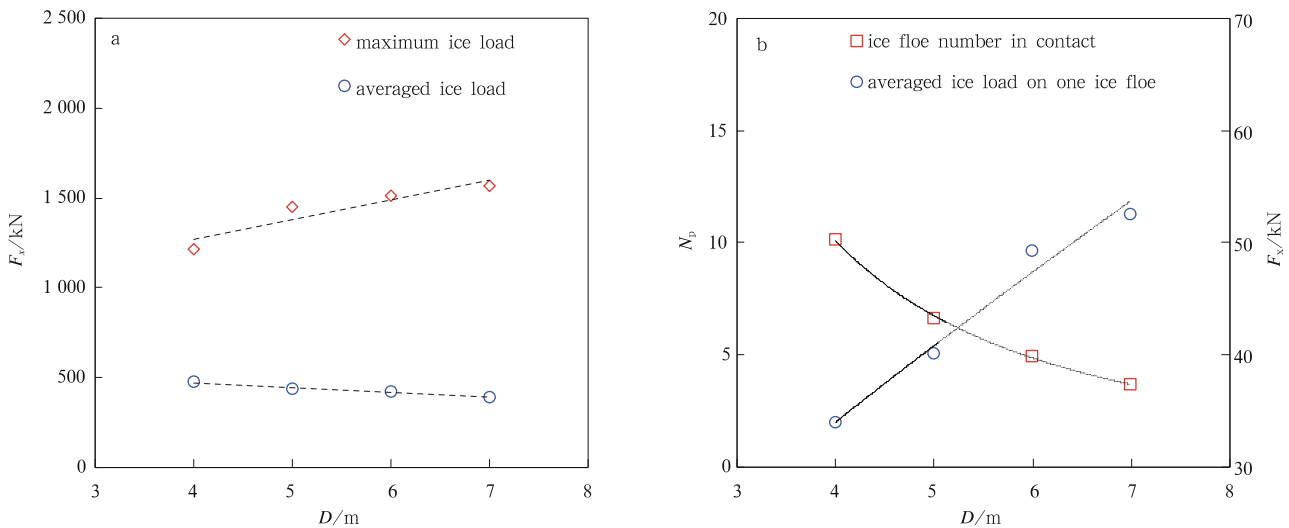
Fig.15. Influence of ice floe size on the ice load on the ship hull. a. Maximum and averaged global ice load and b. contact number and mean load of one ice floe.

contact number are plotted in Fig. 15b. It shows the mean contact force of one ice floe increases obviously with the increase of floe size, whereas the contact number on the hull decreases considerably. Their product, i.e., the global ice resistance, is independent of the floe size when the ice concentration is constant.

    To validate the rationality of this DEM and the simulated ice load on the ship hull, it is necessary to compare the simulated results with the field measured data on icebreaker *Xuelong*. However, the field measurement on the ship hull was not performed in China. Here, we compare the present DEM results with other existing filed data and related numerical results. Frederking (2010) analyzed the influence of ship speed, ice concentration and floe size on the ice resistance to the icebreaker *CCGS Louis S.St-Laurent* based on field measurement of ice load in the Gulf of St. Lawrence. The results show that ice impact forces increase with the increasing of ice floe mass, ice concentration and ship speed. The maximum ice load on the ship

hull is in the range from 0.1×10^3 to 1.8×10^3 kN, which is close to the present DEM results. Recently, Sayed and Kubat (2011) developed a Lagrangian-Eulerian hybrid model to simulate the ice load on the *CCGS Louis S. St-Laurent*. The simulated ice load also increases with the increase of ice thickness and ship speed. The averaged ice load is about 500 kN with an ice thickness of 1.0 m, a ship velocity of 4.0 m/s and an initial ice concentration of 70%. Our simulated result is 630 kN with the same parameters except the concentration of 60%. Although it is a little higher than that obtained by Sayed and Kubat (2011), they are in the same order of magnitude. Wang and Derradji-Aouat (2011) simulated the ice load on the floating system Kulluk of pack ice floes under different ice concentrations. The ice load increases with the increases of ice concentration following a bilinear function. This relationship was also verified with field data. In this study, we also obtained the same relationship, as shown in Fig. 13a. Meanwhile, based on the full-scale measurement data obtained on board of *KV Svalbard* in 2007, Suyuthi et al. (2011) found the

ship resistance increases with the ship speed linearly. The ice resistance is about 2.0×10^3 kN with the ice velocity of 4.0 m/s and the ice thickness of 0.55 m. In this study, the simulated ice resistance is also in this range, as shown in Fig. 10. Moreover, Su et al. (2010) simulated the ice loads on the icebreaker *AHTS/IB*. Although the simulation was performed for level ice, the results can be referred to verify the present DEM results. The maximum and averaged ice loads have the same order of magnitude with the results of this study. With the above comparisons, we can conclude the present results compared well with the existing field data and other numerical results. Although the ship structures are quite different, the relationships between the ice load and the ice thickness, the ice concentration and the ship speed are quite consistent. The magnitude of ice load simulated in this study is also in the rational range. Therefore, the present DEM is appropriate to simulate the ice load on a ship hull. The influence of the ice parameters and the ship speed on the ice load can also be analyzed qualitatively.

5 Conclusions

Interactions between ice floes and the ship hull are simulated to determine the global ice loads on the ship hull using the DEM in broken ice fields. The ice floe is modeled with a 3D dilated disk, and the ship hull is constructed with overlapped 3D disks. The influences of ship maneuvering speeds and ice conditions (current velocity and direction, ice thicknesses, floe sizes, concentration) on the global ice resistance are discussed based on the DEM results. The ice load increases with the increase of ship speed, current velocity, ice concentration and ice thickness. But the influence of ice floe size is not obvious under constant concentration. The simulated results are compared with the existing numerical data and field measurement data. Although the sea ice parameters and the ship hull structure are not exactly the same, the magnitude of ice load on the ship hull and the relationships between the ice load and the ice parameters are quite consistent. The simulation results can still indicate the influence of ice conditions on the ice resistance in spite of some simplifications and assumptions.

In the next studies, the geometric structure of the ship hull and the irregular shape of ice floes will be developed exactly to improve the precision of DEM results. More ship maneuvering performances (turning and zig-zag maneuvers) will be performed to study the ice load. Moreover, the freezing effect between ice floes will also be considered to analyze the impact of level ice on the ship hull.

Acknowledgements

References

Aksnes V. 2010. A simplified interaction model for moored ships in level ice. Cold Regions Science and Technology, 63: 29–39

Dai M, Shen H H, Hopkins M A, et al. 2004. Wave rafting and the equilibrium pancake ice cover thickness. Journal of Geophysical Research, 109: C07023

Frederking R. 2010. Ice loading on a ship in discontinuous ice. In: Proceedings of the Twentieth International Offshore and Polar Engineering Conference, Beijing, China. Cupertino: The International Society of Offshore and Polar Engineers (ISOPE), 1188–1195

Hansen E H, Loset S. 1999a. Modelling floating offshore units moored in broken ice: model description. Cold Regions Science and Technology, 29: 97–106

Hansen E H, Loset S. 1999b. Modelling floating offshore units moored in broken ice: comparing simulations with ice tank tests. Cold Regions Science and Technology, 29: 107–119

Hopkins M A. 1998. Four stages of pressure ridging. Journal of Geophysical Research, 103: 21883–21891

Hopkins M A. 2004. Discrete element modeling with dilated particles. Engineering Computations, 21: 422–430

Hopkins M A, Shen H H. 2001. Simulation of pancake-ice dynamics in wave field. Annals of Glaciology, 33: 355–360

Karulin E B, Karulina M M. 2011. Numerical and physical simulations of moored tanker behaviour. Ship and Offshore Structures, 6(3): 179–184

Konno A. 2009. Resistance evaluation of ship navigation in brash ice channels with physically based modeling. In: Proceedings of the 20th International Conference on Port and Ocean Engineering under Arctic Conditions. Luleå, Sweden: Lulea University of Technology, POAC09-105

Kujala P, Arughadhoss S. 2012. Statistical analysis of ice crushing pressures on a ship's hull during hull-ice interaction. Cold Regions Science and Technology, 70: 1–11

Lau M, Lawrence K P, Rothenburg L. 2011. Discrete element analysis of ice load on ships and structures. Ships and Offshore Structure, 6(3): 211–221

Lepparanta M, Lensu M, Lu Q M. 1990. Shear flow of sea ice in the Marginal Ice Zone with collision rheology. Geophysica, 25(1–2): 57–74

Liu Z, Amdahl J. 2010. A new formulation of the impact mechanics of ship collisions and its application to a ship-iceberg collision. Marine Structures, 23(3): 360–384

Liu Z, Amdahl J, Løset S. 2011. Plasticity based material modelling of ice and its application to ship-iceberg impacts. Cold Regions Science and Technology, 65(3): 326–334

Løset S, Kanestrøm Ø, Pytte T. 1998. Model tests of a submerged turret loading concept in level ice, broken ice and pressure ridges. Cold Regions Science and Technology, 27: 57–73

Polojarvi A, Tuhkuri J. 2009. 3D discrete numerical modelling of ridge keek punch through tests. Cold Regions Scienc and Technology, 56: 18–29

Sawamura J, Tachibana T. 2011. Development of a numerical simulation for rotating and sliding of the ice floes along a ship hull. In: Proceedings of the 21st International Conference on Port and Ocean Engineering under Arctic Conditions. Montreal, Canada: Curran Associates Inc, POAC11-036

Sayed M, Kubat I. 2011. Forces on ships transiting pressured ice covers. In: Proceedings of the 21st International Offshore and Polar Engineering Conference. Hawaii, USA: The International Society of Offshore and Polar Engineers (ISOPE), 1087–1092

Selvadurai A P S, Sepehr K. 1999. Two-dimensional discrete element simulations of ice-structure interaction. International Journal of Solids and Structures, 36: 4919–4940

Shen H H, Hibler W D, Lepparanta M. 1987. The role of floe collisions in sea ice rheology. Journal of Geophysical Research, 92(C10): 7085–7096

Su B, Riska K, Moan T. 2010. A numerical method for the prediction of ship performance in level ice. Cold Regions Science and Technology, 60(3), 177–188

Su B, Riska K, Moan T. 2011. Numerical simulation of local ice loads in uniform and randomly varying ice conditions. Cold Regions Science and Technology, 65: 145–159

Sun S, Shen H H. 2012. Simulation of pancake ice load on a circular cylinder in a wave and current field. Cold Regions Science and Technology, 78: 31–39

Suyuthi A, Leira B J, Riska K. 2011. Full scale measurement on level ice resistance of icebreaker. In: Proceedings of the ASME 30th International Conference on Ocean, Offshore and Arctic Engineering (OMAE2011), Rotterdam, The Netherlands. Rotterdam: The American Society of Mechanical Engineers (ASME), OMAE2011-50066

Suyuthi A, Leira B J, Riska K. 2012. Statistics of local ice load peaks on ship hulls. Structural Safety, 40: 1–10

Wang J, Derradji Aouat A. 2011. Numerical assessment for stationary structure (Kulluk) in moving broken ice. In: Proceedings of the 21st International Conference on Port and Ocean Engineering under Arctic Conditions, Montreal, Canada. Montreal: Curran Associates Inc, POAC11-172

Xu Z, Tartakovsky A M, Pan W. 2012. Discrete-element model for the interaction between ocean waves and sea ice. Physical Review E, 85: 016703

Zhan D, Agar D, He M, et al. 2010. Numerical simulation of ship ma-neuvering in pack ice. In: Proceedings of the ASME 2010 29th International Conference on Ocean, Offshore and Arctic Engineering, Shanghai, China. Shanghai: The American Society of Mechanical Engineers (ASME), OMAE2010-21109

Zhou L, Riska K, Polach R B, et al. 2013. Experiments on level ice loading on an icebreaking tanker with different ice drift angles. Cold Regions Science and Technology, 85: 79–93

Zhou L, Su B, Riska K, et al. 2012. Numerical simulation of moored structure station keeping in level ice. Cold Regions Science and Technology, 71: 54–66